ADVANCED BIOLOGY
www.advanced-bio.com

Inertial Microfluidic Purification of CAR-T-Cell Products

*Mona T. Elsemary, Michelle F. Maritz, Louise E. Smith, Majid Warkiani, Veronika Bandara, Silvana Napoli, Simon C. Barry, Justin T. Coombs, and Benjamin Thierry**

Chimeric antigen receptor T (CAR-T) cell therapy is rapidly becoming a frontline cancer therapy. However, the manufacturing process is time-, labor- and cost-intensive, and it suffers from significant bottlenecks. Many CAR-T products fail to reach the viability release criteria set by regulators for commercial cell therapy products. This results in non-recoupable costs for the manufacturer and is detrimental to patients who may not receive their scheduled treatment or receive out-of-specification suboptimal formulation. It is demonstrated here that inertial microfluidics can, within minutes, efficiently deplete nonviable cells from low-viability CAR-T cell products. The percentage of viable cells increases from 40% (SD ± 0.12) to 71% (SD ± 0.09) for untransduced T cells and from 51% (SD ± 0.12) to 71% (SD ± 0.09) for CAR-T cells, which meets the clinical trials' release parameters. In addition, the processing of CAR-T cells formulated in CryStor yields a 91% reduction in the amount of the cryoprotectant dimethyl sulfoxide. Inertial microfluidic processing has no detrimental effects on the proliferation and cytotoxicity of CAR-T cells. Interestingly, ≈50% of T-regulatory and T-suppressor cells are depleted, suggesting the potential for inertial microfluidic processing to tune the phenotypical composition of T-cell products.

1. Introduction

Chimeric antigen receptor T (CAR-T) cell therapy is a transformative cancer therapy. Currently, there are four Food and Drug Administration (FDA)-approved CAR-T-cell-based products, Kymriah (Novartis) and Yescarta (Gilead/Kite Pharm), Tecartus (Kite Pharm), and Breyanzi (Juno Therapeutics/Bristol Myers Squibb).[1–3] Many more CAR-T cell formulations are currently at the investigational stage, with over 500 clinical trials underway targeting various cancers.[4] However, the CAR-T cell manufacturing process is hampered by several significant barriers, which contribute to high cost of goods and likely in suboptimal clinical outcomes. These issues impede the fulfillment of CAR-T immunotherapy full potential.[4] Identified manufacturing challenges include 1) a significant variability in the starting material, due to either substantial differences in patients' cell composition or use of different cell collection/enrichment methods; 2) the limited scalability of virus-based genetic modification; 3) the inherent need for long ex vivo expansion times to produce sufficient cell numbers for a clinical dose; and 4) the cryopreservation of the final cellular product, which can affect both cell viability and functionality.[5] The need to address these manufacturing barriers has driven intensive research; including toward shifting from the current centralized and labor-intensive manufacturing model to more decentralized ones, for example, using integrated and semiautomated devices set up on site at the clinical providers.

Of specific practical importance to the CAR-T cell industry is the presence of nonviable cells and debris in a final product, a somewhat inevitable consequence of the complex CAR-T cell

---

M. T. Elsemary
Future Industries Institute
ARC Centre of Excellence in Convergent Bio-Nano Science and Technology
Cell Therapy Manufacturing Cooperative Research Centre
University of South Australia Mawson Lakes Campus
Mawson Lakes, SA 5095, Australia

M. F. Maritz, B. Thierry
Future Industries Institute
ARC Centre of Excellence in Convergent Bio-Nano Science and Technology
University of South Australia Mawson Lakes Campus
Mawson Lakes, SA 5095, Australia
E-mail: benjamin.thierry@unisa.edu.au

L. E. Smith
Future Industries Institute
Cell Therapy Manufacturing Cooperative Research Centre
University of South Australia Mawson Lakes Campus
Mawson Lakes, SA 5095, Australia

M. Warkiani
School of Biomedical Engineering
University of Technology Sydney, Broadway
Ultimo, NSW 2007, Australia

V. Bandara, S. Napoli, S. C. Barry
Women's and Children's Hospital
Adelaide, SA 5006, Australia

J. T. Coombs
Carina Biotech
Adelaide, SA 5095, Australia

The ORCID identification number(s) for the author(s) of this article can be found under https://doi.org/10.1002/adbi.202101018.

DOI: 10.1002/adbi.202101018

manufacturing process. The presence of dead cells can exacerbate side effects, such as fever in patients.[6] To address this issue, the FDA has set a viability criteria for CAR-T products, i.e., at least 80% viable cells in a commercial product and 70% viability in the context of clinical trials. Despite these regulations, substantial numbers of patients still receive out-of-spec treatment below the viability threshold. For example, according to the American Society of Hematology, 29 out of 102 lymphoma and 14 of 92 leukemia patients were treated with a low viability Kymriah/Novartis CTL019 product. While there was no obvious relationship between CTL019 product viability and clinical outcomes in this cohort,[7] Novartis cannot charge for such out-of-spec products. It is also important to note that the majority of patients in this study received a CAR-T cell product with a viability in the range of 70–80%. Evaluation of CAR-T cell products with lower viability (e.g., <70%) should be more comprehensively evaluated,[8] considering the increased potential for inflammation and risk of allergic reactions.[9,10] Improving the viability of these CAR-T products is challenging as while cellular debris can be removed by centrifugation, nonviable cells are harder to remove, especially at the point of care prior to administration to patients.

Conversely, cryoprotectants such as dimethyl sulfoxide (DMSO) are required for the freezing and storage of CAR-T and other cellular products. However, the presence of cryoprotectants can cause severe allergic reactions and toxic side effects in some patients. It is therefore preferable to remove or at least reduce the cryoprotectant concentration in the final product.[11,12] Current commercial CAR-T cell products contain DMSO, at a concentration of 7.5% v/v for Kymriah and 5% v/v for Yescarta, according to their respective FDA package inserts.

Commercially available techniques for the removal of dead cells include Ficoll separation[13] and dead cell removal bead kits or buoyancy-based separations that use specific antibodies for binding to apoptotic markers on the membrane of dead cells.[14,15] Despite their merits, these approaches have limited efficiencies and are also typically associated with significant loss of cells. Several noteworthy newer approaches have been proposed for the separation of dead cells including microfluidic enabled ones such as the use of dielectrophoretic focusing,[16] deterministic lateral displacement (DLD),[17] acoustophoresis,[18] hydrodynamic cell sorting,[19] and inertial microfluidics.[20] Spiral inertial microfluidics has several advantageous features toward implementation in cell therapy manufacturing. Inertial microfluidics using spiral microchannels enables high-throughput fractionation of a cellular suspension based on the cells' physicochemical features (size, shape, and deformability). Inertial microfluidic cell separation is a gentle process, which has been utilized previously in several applications, such as the separation of circulating tumor cells (CTCs) and circulating fetal cells from blood, and the enrichment of other cell types.[21–26] Importantly, it has been shown to have minimal impact on cells. Building on the initial report by Kwon et al.[20] of the potential of inertial microfluidics to deplete nonviable cells from a model cell suspension, we endeavored to investigate its potential in the CAR-T cell manufacturing field. We demonstrate that, under optimal conditions, processing through inertial microfluidic devices significantly increases the percentage of viable cells in CAR-T cell products by removing dead cells and debris effectively. In addition, the process also significantly reduces the amount of cryoprotectant in the final formulation. To assess the clinical relevance, we also demonstrated that the microfluidic purification process had no negative effects on the CAR-T cell function, preserving their proliferation potential and cytotoxic actions. Owing to the cost-effective nature of microfluidics and its ease of automation,[27] inertial microfluidic point-of-care purification could be used at the treating hospital for improving CAR-T cell products prior to infusion to the patients. We anticipate that the implementation of this simple purification step would also enable in many cases the salvage of out-of-specification products, benefiting both patients and manufacturers.

2. Experimental Section

2.1. Fabrication of the Microfluidic Device

An eight-turn polydimethylsiloxane (PDMS) spiral microchannel device (inner radius = 0.8 cm, outer radius = 1.8 cm, channel height = 130 µm, and channel width = 500 µm) was designed, comprising of two inlets and six outlets as shown in **Figure 1**. The sample inlet was used to inject the cellular suspension, while the sheath inlet was used to inject the sheath solution. The SU-8 mold for casting the PDMS device was fabricated by photolithography at the Australian National Fabrication Facility (ANFF University of South Australia, Adelaide). The PDMS devices were prepared by pouring a mixture of the base and curing agent (Sylgard 184, Dow Corning Inc.) at a 10:1 ratio into the SU-8 mold, degassing, and then curing at 60 °C as described previously.[23] Once cured, the PDMS devices were released from the molds and bonded to glass slides using air plasma (Harrick Plasma, USA) at a pressure of 800 Torr for 3 min.

2.2. CAR-T and Untransduced T Cells

Low-viability human CAR-T cells as well as untransduced donor-matched control T cells were obtained from Carina Biotech Pty. Ltd., under the ethics approval number IBC0141. The model CAR-T cells were healthy donor T cells that were lentivirally transduced with a second-generation proprietary CAR against a tumor-associated antigen. The cryovials were transferred from the manufacturing laboratory on dry ice and stored at −80 °C/liquid nitrogen until used. Thawing was performed rapidly with gentle agitation in a 37 °C water bath. The cells were then either washed and resuspended in phosphate buffered saline (PBS) + 1% fetal bovine serum (FBS) (Life Technologies, Australia) at a total cell concentration of 7×10^6 cells mL^{-1} for initial optimizations, or thawed in Cryostor without washing and introduced into the microfluidic device through the cell suspension inlet.

2.3. Separation in Microfluidic Device

The microfluidic device was connected to a syringe pump, which controlled the inlets' flow rates, as depicted in Figure 1.

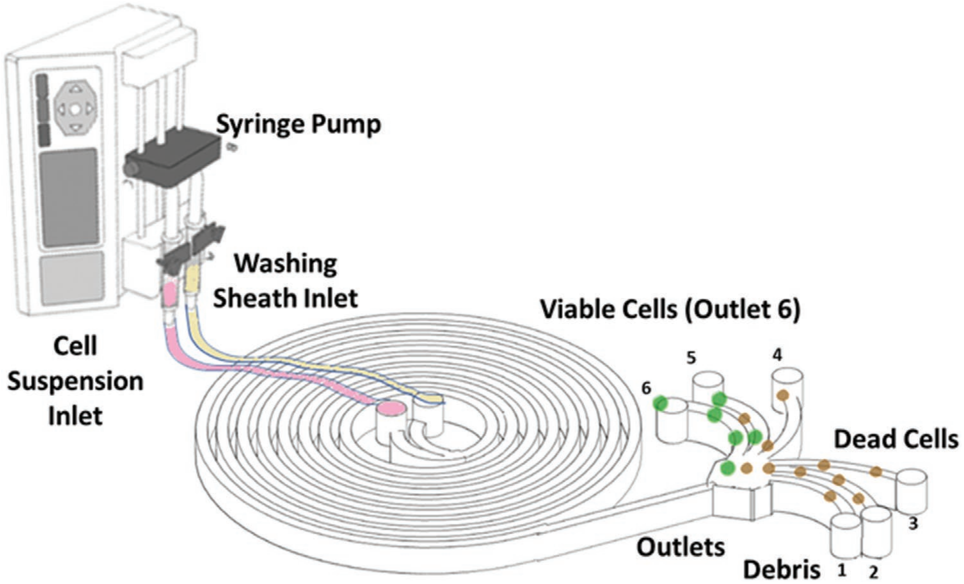

Figure 1. Schematic representation of the design and operation of the inertial microfluidic device. Viable (larger) cells are collected in the inner most outlet 6, while nonviable cells are collected in outlets 2–5 and debris in outlet 1.

Optimization for inlet flow rates was first performed using cell-free PBS containing 10% DMSO (Sigma–Aldrich, Australia), (a concentration typically used for cryopreservation protocols for hematopoietic cell products). Flow rates were then optimized with Raji cell line (CCL-86, ATCC, USA) resuspended in PBS + 1% FBS + 10% DMSO at a concentration of 1×10^6 cells mL^{-1}. CAR-T cells resuspended in PBS + 1% FBS + 10% DMSO (at a concentration of 7×10^6 cells mL^{-1}) were then used to confirm that the optimized separation protocols worked for primary human T cells. Separation in the microfluidic device was performed at a flow rate of 1 mL min^{-1} and fed with PBS + 1% FBS from the sheath inlet, set at the same flow rate (1:1 flow rate ratio), as shown in the schematic representation in Figure 1. The enriched viable cellular fraction (larger cells) was collected in the inner outlet (outlet 6), while dead cells and debris were collected in the outer outlets of the device. Further optimization was performed using cells suspended in Cryostor, at the cell concentration described in the following sections. Cells were separated in the microfluidic device at a flow rate of 1 mL min^{-1}; however, plasmalyte +5% bovine serum albumin (BSA) was fed from the sheath inlet, at the same flow rate. Different flow rates and flow rate ratios for the two inlets were tested to optimize the device performance. The processed cells were collected in the outlets of the device. The volumes were measured, and cells collected by centrifugation at 500 × *g* for 5 min and analyzed for viability and phenotypes. The percentage of DMSO was measured before and after device processing.

2.4. Cell Viability Measurements and Cell Size Distributions

The viability of cell suspensions was assessed by manual cell count on a hemocytometer using the trypan blue exclusion assay using trypan blue 0.4% solution (Thermo Fischer Scientific, Australia). Cell size distributions were determined by staining for CD3, using antihuman CD3 fluorescein isothiocyanate (FITC) (clone SK7) (Life Technologies, Australia) and propidium iodide (PI) exclusion for gating of dead cells. Data were collected on the imaging flow cytometer (ImageStreamx Mark II, AMNIS, Seattle, WA, USA). Analysis of the cellular populations was performed with the IDEAS software Version 6.1 (AMNIS, Seattle, WA, USA) and FlowJo V10 (FLOWJO, USA). Cell size distributions were calculated using an adaptive erode mask (M04 CH04 77) on the AMNIS software, which allows an accurate calculation of cell diameters. Percentage recovery, depletion and viability were calculated as follows

$$\text{Percentage recovery of viable cells} \\ = \frac{\text{Total number of viable cells collected in outlet 6}}{\text{Total number of viable cells collected in all outlets}} \tag{1}$$

$$\text{Percentage depletion of dead cells} \\ = \frac{\text{Total number of dead cells collected in depletion outlets } 1-5}{\text{Total number of dead cells collected in all outlets}} \tag{2}$$

$$\text{Percentage viability} = \frac{\text{Number of viable cells}}{\text{Total number cells}} \tag{3}$$

2.5. CAR-T Cell Phenotyping

Cells were stained for surface markers and visualized using an imaging flow cytometer (ImageStreamx Mark II, AMNIS, Seattle, WA, USA). T cells were stained with antihuman CD3 FITC (clone SK7) or antihuman CD3 BV421 (clone UCHT1), and phenotypes were characterized using antihuman CD45RO PE (clone UCHL1), CD45RA PerCP-CY 5.5 (clone HI 100), CD4 EF450 (clone SK3), CD8A PECYN5.5 (clone RPA-T8) (Life Technologies, Australia), CCR7 BV421 (clone 150503) (BD Life

Sciences, Australia), CD25 PE-Cy7 (clone M-A251) (BD Life Sciences, Australia), and CD4 FITC (clone OKT4) (Biolegend, Australia). The cells were also stained with FOXP3 Alexa Fluor-647 (Biolegend, Australia) after fixation and permeabilization using the FOXP3 fixation and permeabilization buffer set (Biolegend, Australia) as per the manufacturer's instructions. The gating strategies and controls used are shown in Figures S4–S8 (Supporting Information).

2.6. DMSO Measurements before and after Device Processing Using UV–Vis Spectrophotometry and Capillary Electrophoresis

DMSO concentrations in solutions before and after processing were determined initially by UV–vis spectrophotometry using a Thermo Evolution 201 UV–VIS spectrophotometer (Thermo Fisher, Australia), according to previously established methods.[28] The $\lambda_{\max}$ for DMSO absorption was 209 nm.[29] A calibration curve at 209 nm was created using serial dilutions of a DMSO stock solution at (10% v/v) diluted in PBS and was found to be linear across a narrow concentration range from 0.01 to 0.07% v/v. The DMSO concentration in PBS was measured after centrifugation and removal of the cells. The DMSO concentrations were serially diluted in PBS to fall in the linear range of the calibration curve. The % v/v DMSO in each outlet and the % removal were calculated. For experiments involving cells suspended in Cryostor and washed with plasmalyte/BSA, the BSA interfered with the DMSO UV–vis measurements so capillary electrophoresis was used to separate DMSO from BSA. The separation was performed on an Agilent 7100 (Agilent Technologies, Waldbronn, Germany) with a diode array detector monitoring at the $\lambda_{\max}$ of 209 nm for DMSO. Fused silica capillaries (50 µm i.d., 360 µm o.d.) were obtained from Polymicro (Phoenix, AZ, USA). The capillary length was 48 cm with a 39.5 cm effective length. The capillary was pretreated prior to use by flushing with 1 M NaOH, followed by water, and then the background electrolyte (BGE) for 20 min each. The sample was injected by applying 17 mbar of pressure for 8 s (≈10 nL in 130×10^{-3} M NaOH) followed by BGE, injected in the same manner. Between each sample, the capillary was flushed with BGE for 10 min. At the end of a series of injections, the capillary was flushed for 1 min with 1 M NaOH, 10 min with water, and 10 min with air. DMSO and BSA peaks were detected by capillary electrophoresis using borate buffer. Calibration curves of DMSO and Cryostor were generated at 209 nm using serial dilutions in the presence and absence of plasmalyte/BSA, as shown in Figure S1 (Supporting Information). Integration was performed on the Agilent software (Agilent Technologies, Waldbronn, Germany) on electropherograms and corrected for the electrophoretic mobility by dividing the area of the peak by the migration time.

2.7. Cell Proliferation Assay

Cell proliferation was determined by staining with the proliferation dye, carboxyfluorescein succinimidyl ester (CFSE) (Biolegend, Australia), as per the manufacturer's guidelines. Leukocytes (2×10^6 cells mL^{-1}) were resuspended in PBS and labeled with 10×10^{-6} M CFSE for 10 min at 37 °C. The reaction was stopped by adding an equal volume of FBS and incubated for 2 min at room temperature. The cells were then washed twice and the CFSE-labeled cells were cultured for 48 h at 37 °C and 5% CO_2 in 96-well microtiter plates in complete X-vivo medium (X-Vivo 15 (Lonza, Australia)), 5% inactivated human serum (Life Technologies, Australia), and 1% glutamate (Life Technologies, Australia)). To stimulate the proliferation of the CAR-T and untransduced cells, the cells were activated using anti-CD3-coated plates (5 µg mL^{-1}) and soluble anti-CD28 (4 µg mL^{-1}) and interleukin 2 (500 U mL^{-1}) (Life Technologies, Australia). Proliferation was compared between cells after device processing at 3 and 7 days. T cells were gated for viability using CD3 staining and PI exclusion (0.1 mg mL^{-1}), and proliferation analysis was performed using the imaging flow cytometer. The proliferation index was calculated as the cells in all generations, including the parental, divided by the number of original parent cells at the start of the experiment.

2.8. Cytotoxicity Assay

The CAR-T and untransduced cells were co-cultured with the PC-3-Luc2 cancer cell line (ATCC CRL-1435-LUC2, ATCC, USA) at different ratios (30:1, 3:1, and 1:1) and cultured for 16 h in 96-well plates in complete X-vivo medium. The cytotoxicity assays were normalized using the same number of processed and nonprocessed viable cells. Luciferase assays were performed with Bright-Glo Luciferase Assay System (Promega, Australia) and performed according to the manufacturer's protocol. Briefly, 100 µL of Brightglo reagent was added to cells grown in 100 µL of medium and after complete cell lysis, the 200 µL mix was transferred to an opaque 96-well plate and luminescence measured using a Glomax Explorer luminometer (Promega, Australia). Each experiment was done in triplicate, and the cytotoxicity percentage was calculated using Equation (4)

$$\text{Percentage cytoxicity} = 100 - \left[\frac{(\text{experimental cytolyis} - \text{media only})}{(\text{maximum cytolyis} - \text{media only})} \times 100 \right] \tag{4}$$

2.9. Statistical Analysis

All experiments were repeated at least three times, and data were analyzed nonparametrically using GraphPad Prism 8.0 (GraphPad Software, Inc.), which were used to calculate the two-sided *p*-values as well as generate all graphs. Flow cytometry data were exported initially into an excel sheet from FlowJo and then analyzed statistically with GraphPad Prism. The data were analyzed using paired two-way analysis of variance (ANOVA) mixed model followed by Tukey multiple comparison test for multiple variable experiments. For single variable experiments, nonparametric Wilcoxon paired *T*-test was used. No exclusion of statistical outliers was applied.

3. Results and Discussion

3.1. Inertial Microfluidic Enrichment of Viable CAR-T Cells

An inertial microfluidic spiral device was designed and adapted from previous studies[23,30,31] and fabricated using soft lithography. The device comprises two inlets for the cell suspension and sheath buffer, respectively, and six outlets from which the fractionated cell suspensions are collected. The device was connected to a syringe pump via its two inlets. The larger cellular fraction is enriched in the inner outlet #6, while debris is mostly found in the outer outlet #1. The total flow rate, inlets' flow rate ratios, microfluidic channel dimensions, and the resistance of outlets are the key parameters that can be modified to optimize the cell-fractionation process. The device operation was first optimized using Raji cells to optimize the flow rates and DMSO removal from the cell suspension, as shown in Figure S1e,f (Supporting Information). To investigate the potential of inertial microfluidics to more finely separate viable from dead CAR-T cells, we first determined the respective size distributions of a batch of human CAR-T cells and donor-matched untransduced T cells using imaging flow cytometry (Figure S5, Supporting Information). It was observed that viable expanded T cells in both the CAR-T and untransduced control samples had larger mean cell diameters compared to dead cells (8 ± 0.07 µm vs 7 ± 0.07 µm; **Figure 2**). Cells typically undergo death through either apoptosis or necrosis. While the apoptotic pathway typically involves a shrinkage of the cells, the necrotic pathway involves cell swelling.[32] For ex-vivo-expanded CAR-T cells, T-cell exhaustion and apoptosis are expected to occur to some extent depending on the cytokines and activation conditions used,[33–36] which could explain the observed size difference between nonviable and viable CAR-T cells. The modest yet significant difference in size between viable and nonviable T cells suggested the feasibility of enriching the viable fraction using inertial microfluidics. In addition, it should be noted that the fractionation of cell suspensions by inertial microfluidics is governed not only by their characteristic dimensions but also by their rigidities.[19,37]

To investigate the possibility of depleting nonviable cells and consequently rescuing batches of CAR-T cells that fall short of the viability threshold, both batches of CAR-T cells, and donor-matched T cells with low viabilities were utilized. The initial percentages of viable cell in these batches as well as in donor-matched untransduced T-cell batches were compared to the percentages following inertial microfluidic processing. The initial T-cell viability of these batches ranged from extremely low (38%) to moderate (58% and 59%)

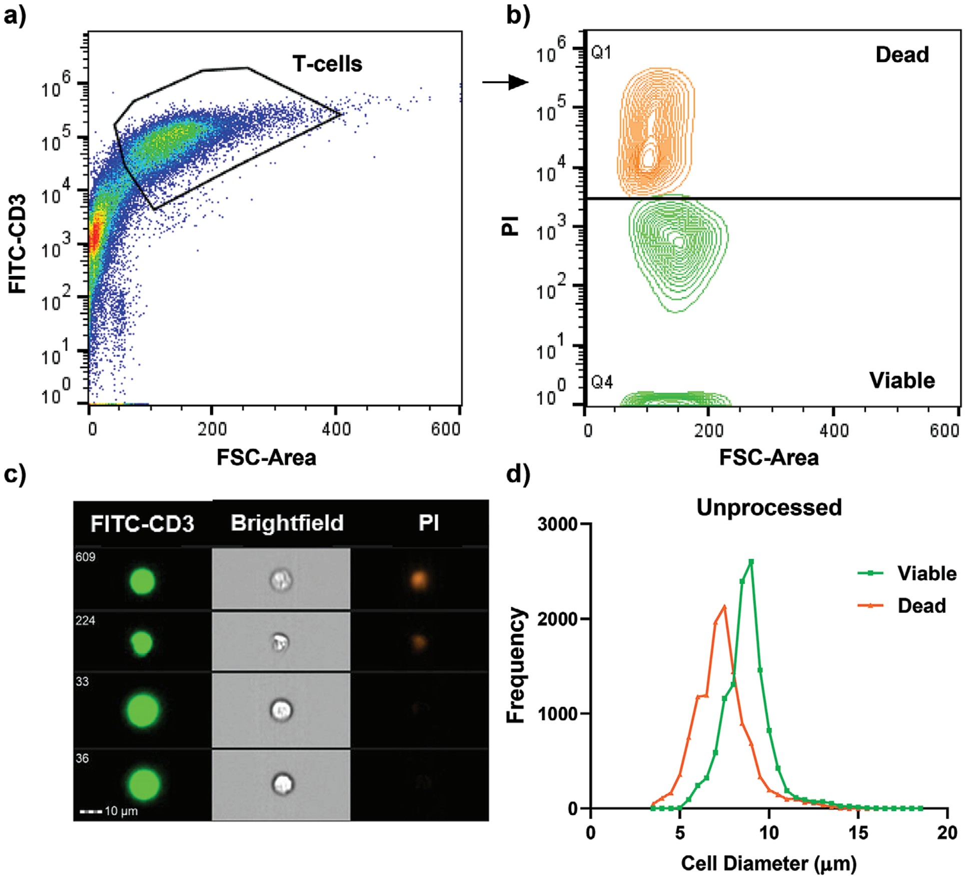

Figure 2. Size distribution of viable and nonviable CAR-T cells. Cells were analyzed using imaging flow cytometry and size distributions were calculated using an adaptive erode mask. a) Gating strategy used. b) Dead versus viable populations as gated using positive permeabilized PI controls and negative nonpermeabilized controls. c) Representative images of viable and nonviable cells. d) Size distribution of viable and nonviable CAR-T cells.

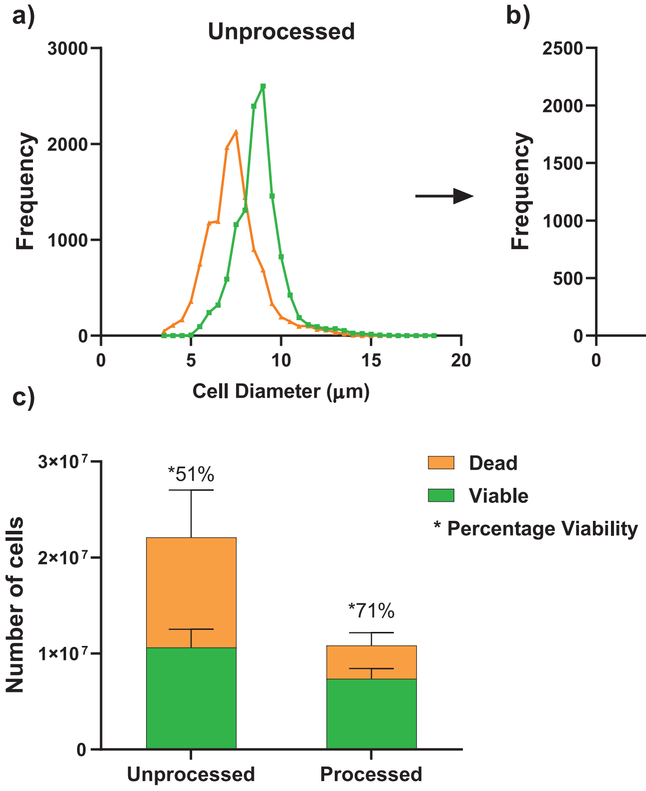

Figure 3. Inertial microfluidic enrichment of viable CAR-T cells suspended in PBS+1% FBS (total cell concentration of 7×10^6 cells mL^{-1}). A sheath flow rate of 1 mL min^{-1} inlet and a flow rate ratio of 1:1 (cellular suspension: sheath) were used. Representative histograms showing the size distribution of viable and nonviable cells a) before and b) after processing. c) Numbers of viable and nonviable cells. The percentage of viable cells (indicated by *) increased significantly for the three tested CAR-T cell batches ($p < 0.05$) (Wilcoxon matched-pairs signed rank *T*-test).

viability. Significant increases in the percentages of viable T cells for all tested batches were observed following inertial microfluidic processing ($p < 0.05$). Nonviable cells were significantly depleted and, as a result, the average percentage of viable T cells of the CAR-T cell batches increased from 51% (SD ± 0.12) before processing to 71% (SD ± 0.09) after processing, corresponding to an ≈25% increase in viability of the product as shown in **Figure 3**c. Importantly, the recovery of viable T cells ranged from 62% to 80% in the tested CAR-T cell batches (average recovery = 70%). Similar results were observed for donor-matched untransduced T cells, with the average percentage of T-cell viability increasing from 40% (SD ± 0.12) to 71% (SD±0.09) after processing with a recovery of viable cells ranging from 66% to 84% (Figure S2a, Supporting Information). An additional viability measurement by staining for CD3 and PI of one CAR-T cell batch yielded a similar increase the percentage of viable cells (from 53% to 70%) and 70% recovery of viable cells, as shown in Figure 3a,b. These results indicate that inertial microfluidics can efficiently deplete nonviable cells from low-viability CAR-T cell products with acceptable recovery of the viable cells. Interestingly, there was no difference in the percentage of CAR positive cells before and after processing (Figure 6b), which indicates that no preferential enrichment or depletion of CAR positive cells over negative ones occurred at the tested conditions. It should be noted a recovery of ≈70% of the viable CAR positive T cells, although superior to commercially available antibody-based kits, could nevertheless be an issue for products with low number of CAR-T cells as these could fail to meet the minimum patient dose.

Following these promising initial results, the performance of inertial microfluidic processing in purifying CAR-T cell products prior to infusion was investigated in a more clinically relevant context. In a common clinical scenario, CAR-T products are frozen at high cell concentration, typically in the range of $(0.6–6.0) \times 10^8$ cells, in 1–3 bags of 10–50 mL volumes, and in presence of cryoprotectant such as Cryostor mixed with other product additives.[38] In clinical trials, the thawed CAR-T cells are usually washed prior to infusion.[34,39] However, in the case of commercial products, the cellular suspensions are typically infused as is and therefore in the presence of substantial amounts of cryoprotectants. This is mostly due to the lack of good manufacturing practice (GMP) compliant facilities for washing and reformulating these products at the point of care.[40] This is significant as the removal of cryoprotectants has been shown to reduce adverse outcomes in patients receiving hematopoietic stem cells.[41,42] We therefore investigated the potential of inertial microfluidics to remove cryoprotectant and reformulate CAR-T cells in a typical infusion agent, such as plasmalyte/BSA. Using CAR-T cells suspended at a total concentration of 7×10^6 cells mL^{-1} in Cryostor and plasmalyte/BSA as the sheath, the feasibility and performance of

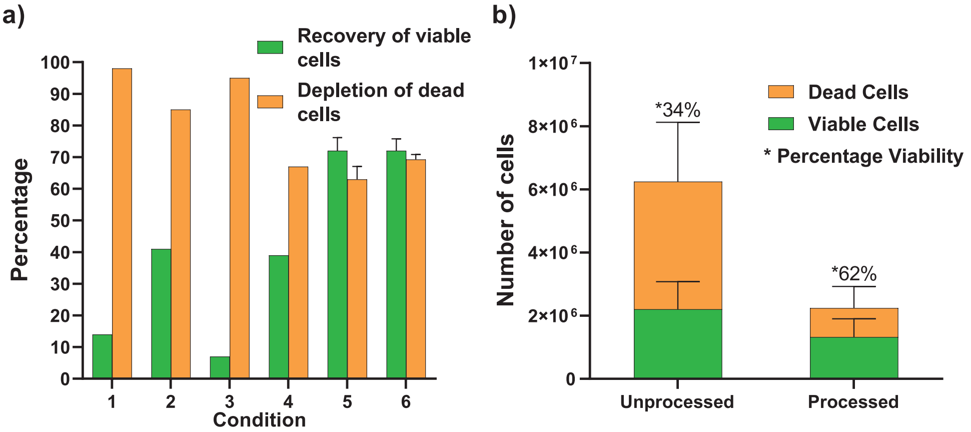

Figure 4. Enrichment of viable CAR-T cells suspended in Cryostor (7×10^6 cells mL^{-1}) and reformulated in plasmalyte+5% BSA. a) Optimization of the recovery of viable cells and depletion of dead cells. Different device configurations, flow rates, and flow rate ratios were tested ($n = 3$): 1) flow rate ratio 1:1, long outlet, sheath flow rate 1 mL min^{-1}; 2) flow rate ratio 1:1, short outlet, sheath flow rate 1 mL min^{-1}; 3) flow rate ratio 1:1, long outlet, sheath flow rate 1.5 mL min^{-1}; 4) flow rate ratio 1:3, short outlet, sheath flow rate 1 mL min^{-1}; 5) flow rate ratio 1:10, long outlet, sheath flow rate 1 mL min^{-1}; and 6) PBS+1% FBS + 10% DMSO, flow rate ratio 1:1, long outlet, sheath flow rate 1 mL min^{-1}. b) Number of viable and nonviable cells before and after processing at an inlet flow rate ratio of Cryostor to plasmalyte/BSA sheath of 1:10 and a sheath flow rate of 1 mL min^{-1}. The percentage viability (indicated by *) increased significantly for CAR-T cells ($n = 4$, $p < 0.05$ with Wilcoxon matched-pairs signed rank *T*-test).

inertial microfluidic purification of a CAR-T cell product prior to patient administration were determined. Using the operating conditions above (sheath flow rate of 1 mL min^{-1}) and a flow rate inlet ratio of 1:1 (cell inlet: sheath inlet), a 98% depletion of nonviable cells was achieved. However, the recovery of viable cells was very low (14%). This drastic reduction in performance was likely due to the large difference in viscosities between Cryostor and plasmalyte/BSA, which prevented efficient mixing of the two inlet streams in the device, as visually observed using dyes. Therefore, several operating conditions using different inlets' flow rate ratios, flow rates, and outlet lengths (used to modulate the pressure inside the device) were tested (as summarized in **Figure 4**a). The effect of the lengths of outlet 6 was tested (long and short). A long outlet provides more resistance to the flow within the device, which was found to yield greater depletion of the smaller sized cells compared to a short outlet length. Using a higher inlet flow rate ratio of 1:10, 72% (SD ± 0.17) and 77% (SD ± 0.19) of the nonviable cells were efficiently removed from the CAR-T cell suspension (Figure 4b) and matched untransduced T cells (Figure S2b, Supporting Information), respectively. This led to an increase in the percentage of viable cells from 34% (SD ± 0.07) to 62% (SD ± 0.15) for CAR-T cells and from 27% (SD ± 0.17) to 44% (SD ± 0.13) for untransduced T cells with 72% (SD ± 0.07) and 69% (SD ± 0.12) recovery of viable cells, respectively.

It should be noted that the concentration of the cell suspension is a key factor in the inertial microfluidic process, and high concentrations can significantly decrease separation efficiencies due to increased cell–cell interactions. This leads to defocusing of the streams and a reduction in inertial focusing efficiency.[12,43] The high CAR-T cell concentration used clinically may contribute to the poor recovery of the viable cells following processing at a 1:1 inlet flow rate ratio. However, with the optimized 1:10 inlet flow rate ratio, rapid mixing occurs in the device, which effectively dilutes the cell suspension.

3.2. Inertial Microfluidic Processing Efficiently Reduces Cryoprotectant in CAR-T Cell Suspensions

To test the capability of the device to reduce DMSO, used as model cryoprotectant, the DMSO concentration in the CAR-T cell collection outlet (outlet 6) before and after inertial microfluidic processing was measured. The DMSO concentration was calculated by establishing a DMSO calibration curve, using UV–vs spectrophotometry. Initial optimization experiments demonstrated that DMSO was diluted in the device. Increasing the sheath flow rate from 1 to 2.5 and 3.5 mL min^{-1} at a constant inlet flow rate ratio of 1:1 reduced the DMSO dilution in the device (Figure S3b, Supporting Information). In contrast, increasing the inlet flow rate ratio diluted the DMSO significantly more. Flow rate ratios of 1:1, 1:2, 1:5, and 1:10 reduced DMSO by 40%, 60%, 70%, and 90% from PBS containing DMSO, respectively (Figure S3b, Supporting Information). However, this was also associated with an increase in the total volume collected. In the microfluidic device used, the outlet volume split ratio is 2:1 (dead cell depletion outlets 1–5: viable cell outlet 6). When processing 1 mL of cell suspension, the volumes collected in the viable cell outlet 6 were, therefore, 0.75, 1, 2, and 3.7 mL for inlets flow rate ratios of 1:1, 1:2, 1:5, and 1:10, respectively. When these conditions were tested with Cryostor in the sample inlet and plasmalyte/BSA as the sheath in the other inlet, consistent mixing and cell focusing occurred only at a flow rate ratio of 1:10 due to the difference in viscosities between the thawed Cryostor cell suspension and the plasmalyte BSA.

To determine the amount of DMSO removal in these sets of experiments, capillary electrophoresis was used to separate the DMSO and BSA peaks, as shown in **Figure 5**a. A calibration curve was first made using peak areas and migration times (Figure S2, Supporting Information). At the flow rate ratio of 1:10, 92% (SD ± 0.01) of the DMSO was removed consistent with complete mixing of the two inlets and resulting dilution of the DMSO initially present in the sample inlet (Figure 5b). The

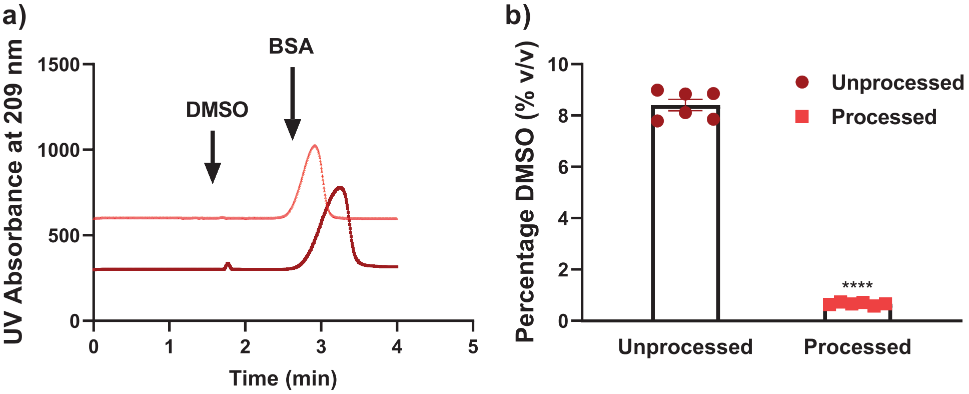

Figure 5. Effect of inertial microfluidics on the depletion of DMSO from cryopreserved T cells in Cryostor. a) DMSO and BSA peaks in capillary electrophoresis. b) Percentage of DMSO before and after device processing with an inlet flow rate ratio of 1:10 (cells in Cryostor: plasmalyte/BSA) ($p < 0.0005$ using paired *T*-test).

processing of a clinically relevant CAR-T cell formulation took 10 min per 1 mL, yielding 3 mL of purified cellular product with an increase in the total viability by ≈25% and a reduction in the concentration of DMSO by greater than 90%. A typical CAR-T cell product is 10–50 mL frozen product containing (0.1–6.0) × 10^8 cells, and it is typically infused at a rate of 10–20 mL min^{-1}. Diluting the product, three times would lead to an increase in infusion volume to 30–150 mL and, therefore, to an increase in the infusion time. Such increased infusion time/volume would still be below the maximum daily intravenous fluid infusion for both adults and children.[44–46] This limitation should be balanced with the increased viability of the CAR-T cells as well as the substantial reduction in the percentage of DMSO.

3.3. Inertial Microfluidic Processing Does Not Affect the Percentage Transduction of CAR-T Cells

Having identified the optimal operating conditions, it was essential to determine the effect of inertial microfluidic processing on the percentage of CAR positive cells in the CAR-T cell product to ensure that there was no specific depletion of CAR positive cells in the CAR-T cell product. To this end, the percentage of transduced CAR-T cells of both $CD4^+$ and $CD8^+$ T-cell populations was assessed before and after device processing. Device processing had no effect on the overall percentage of $CD4^+$ and $CD8^+$ cells (**Figure 6**a). There were also no significant changes to the percentages of CAR positive cells for both $CD4^+$ (59% (SD ± 0.09) vs 60% (SD ± 0.07)) and $CD8^+$ (59% (SD ± 0.17) vs 58% (SD ± 0.18), as shown in Figure 6b.

3.4. Inertial Microfluidic Processing Enriches Central Memory and Stem Cell Phenotypes and Depletes T-Regulatory and T-Suppressor Cells

The phenotypic characteristics of the purified CAR-T cell products were also investigated. It has been reported that the phenotype impacts T-cell longevity and persistence in vivo after transfusion.[47–50] Naive T cells and central memory (CM) T cells have been shown to be longer-lived, and their initial percentage in the transfused product to be directly linked to enhanced clinical outcomes and prognosis. This led to modified ex vivo expansion protocols to increase the desired phenotypes and prevent differentiation to terminally differentiated cells.[51–54] Some protocols selected particular phenotypes by magnetic selection and

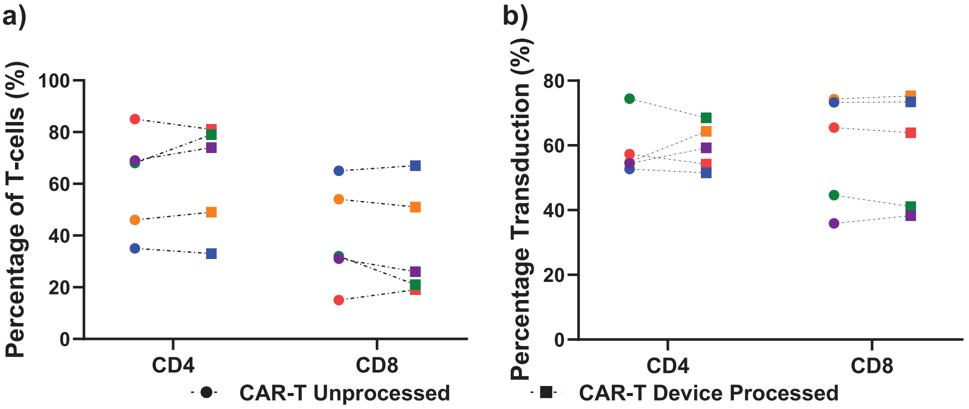

Figure 6. Effect of inertial microfluidic processing on the percentage transduction in $CD4^+$ and $CD8^+$ T cells. a) Percentages of $CD4^+$ and $CD8^+$ T cells. b) Percentage transduction of $CD4^+$ and $CD8^+$ CAR-T cells (each color corresponds to one of the five tested CAR-T suspension).

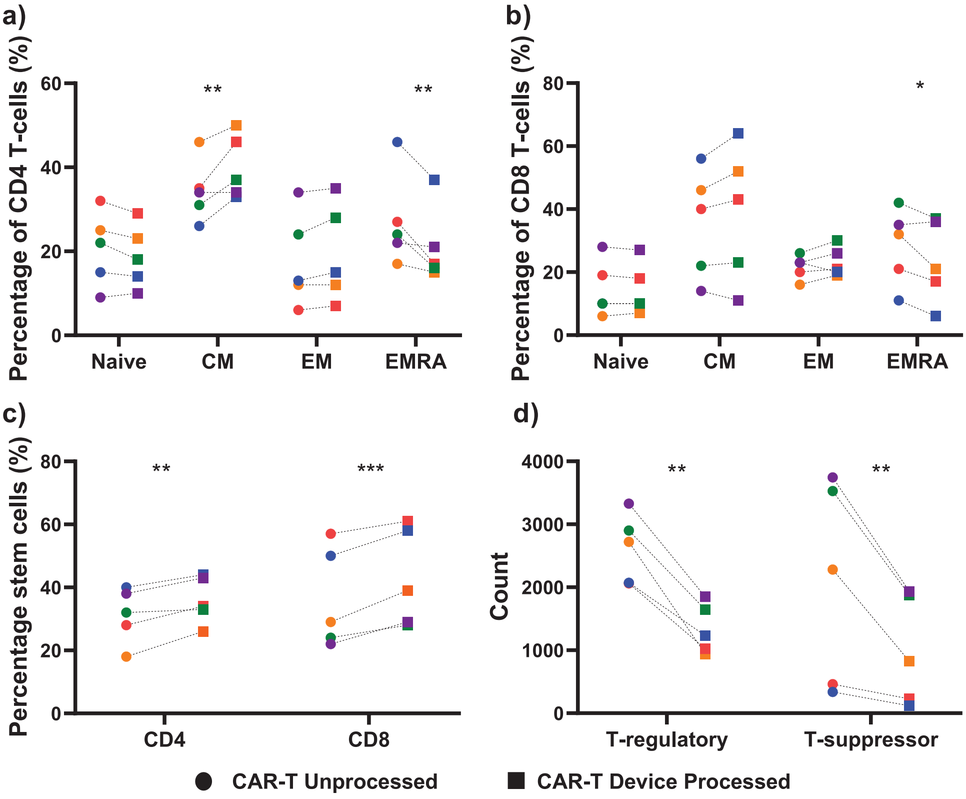

Figure 7. Effect of inertial microfluidic processing on the frequency of CAR-T cells phenotypes. Percentages of naive, central memory (CM), effector memory (EM), and terminally differentiated effector cells (EMRA) for a) CD4 and b) CD8 CAR-T cells. c) Percentages of CD4 and CD8 stem cell phenotype. d) Number of CD4 T-regulatory and CD8 T-suppressor cells ($n = 5$, * $p < 0.05$, ** $p < 0.005$, and ** $p < 0.0005$ using a two-way mixed model ANOVA; each color represents an independent CAR-T cell suspension).

fluorescence-activated sorting (FACS) before CAR-T delivery and cell expansion.[55] To test whether inertial microfluidic processing affected the cellular phenotypes, cells were stained for markers associated with CD4$^+$ helper T cells, CD8$^+$ cytotoxic T cells, central memory T cells (CD45RO$^+$, CCR7$^+$), stem cell T cells (CD45RO$^+$CD45RA$^+$CCR7$^+$), and markers for CD4$^+$T-regulatory cells and CD8$^+$T-suppressor cells (CD25$^+$high, FOXP3$^+$, CD127$^+$ low) and cellular suspensions were analyzed before and after processing. Gating strategies and fluorescence minus one controls are shown in Figures S5–S8 (Supporting Information).

As shown in **Figure 7**, the tested CAR-T cells batches initially contained 56% (SD ± 0.2) CD4$^+$ T cells and 44% (SD ± 0.2) CD8$^+$ cells. As noted above, there was no significant difference in the percentages of CD4$^+$ and CD8$^+$ cells before and after processing, as shown in Figure 6a. Similar results were obtained for the control T cells (Figure S12, Supporting Information). Analyses of the CD4$^+$ phenotypes indicated that there was a small increase in the CM phenotype from 32% (SD ± 0.04) to 38% (SD ± 0.18) for CAR-T cells, with similar increases for the control untransduced T cells ($p < 0.05$; Figure 7a; Figure S12a, Supporting Information). There was also a significant depletion of CD4$^+$ terminally differentiated effector cells (EMRAs) of both the CAR-T cells and control T cells (57% and 45%; $p < 0.005$ and $p < 0.05$, respectively). There was also a small, but consistent increase in CD8$^+$ CM from 41% (SD ± 0.14) to 46% (SD ± 0.17) for CAR-T cells in all five batches (Figure 7b, N.S). The proportion of CD8$^+$ EMRAs were reduced by 55% (SD ± 0.09) for the CAR-T cells ($p < 0.05$).

The stem cell phenotype characterized by CD45RO+/CD45RA+/CCR7+is expressed on both CD4$^+$ and CD8$^+$ cells. A small but consistent and significant increase in the percentage of cells with stem cell phenotypes was found across all batches upon device processing. For CD4$^+$ cells, the percentage increased from 30% (SD ± 0.09) to 34% (SD ± 0.07), while for CD8$^+$ cells, the percentage increased from 40% (SD ± 0.15) to 47% (SD ± 0.15) (Figure 7c). Similar data were obtained for the control T cells (Figure S12c, Supporting Information). After inertial microfluidic processing, there was a depletion of CD4$^+$ T-regs (53% ± 0.11) and CD8$^+$ T-supp cells (54% ± 0.09) (Figure 7d, statistically significant at $p < 0.005$). Clinical blood samples from cancer patients usually have increased numbers of T-regs and T-supp cells, which are immunosuppressive.[56–59] Due to their negative influence on cell proliferation and the exhaustion status of the cells, depletion of T-regs and T-supp cells by magnetic selection is used in the production of some clinical CAR-T products.[60–62] However, the clinical value of depleting these phenotypes during manufacture still needs to be ascertained.

The ability of inertial microfluidic processing to modulate the proportions of various T-cell phenotypes is explained by differences in their average dimensions, as determined using imaging flow cytometry. The CM (7.6 µm SD ± 0.9) and stem cell (8 µm SD ± 0.5) phenotypes had slightly larger diameters compared to other T cells, while the T-reg (6.8 µm SD ± 0.3), T-supp (7.6 µm SD ± 1.1), and EMRA (7 µm SD ± 0.2) phenotypes had smaller diameters.

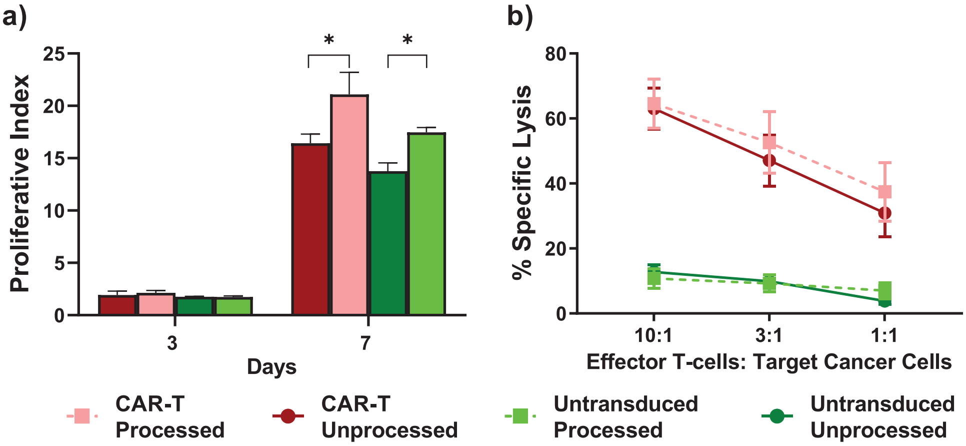

Figure 8. Effects of inertial microfluidic processing on T-cell functionality. a) T-cell proliferation assayed by CFSE staining. Proliferative indexes at days 3 and 7 for both CAR-T cells and control untransduced T cells with or without device processing (*n* = 3). b) Cytotoxicity of CAR-T cells as measured by the percentage specific lysis of CAR-T cells and control untransduced T cells cocultured with PC-3-Luc2 cancer cells expressing the CAR target with and without inertial microfluidic processing (*n* = 3).

3.5. Inertial Microfluidic Processing of CAR-T Cell Product Has No Effect on Proliferation and Cytotoxicity

The process of spiral inertial microfluidic cell size separation has previously been shown to have no detectable effects on cell functionality,[23] likely due to the fairly gentle flow conditions experienced by cells and low residence time inside the devices. Other microfluidic cell sorting technologies have been shown to have minimal effect on T-cell functionality. Most notably, both DLD (GPB Scientific)[63] and acoustophoretic (Draper laboratory)[64] microfluidic devices are presently being implemented in the CAR-T cell manufacturing industry. To confirm the absence of significant deleterious effects on the CAR-T cell functionality and proliferation, a proliferation assay and a cytotoxicity study were performed. After 3 days, no significant differences in proliferation were observed, as indicated by the proliferative index of 2.1 (SD ± 0.6) for processed CAR-T cells compared to 1.7 (SD ± 0.2) for the nonprocessed cells (**Figure** 8a). However, after 7 days, the proliferative index was significantly higher, 19.6 (SD ± 4), for the processed CAR-T cells, compared to 15.6 (SD ± 0.9) for the nonprocessed sample. Similar results were obtained for the untransduced control cells, indicating that device processed cells have a proliferative advantage over the nonprocessed cells at day 7. The significance of this finding and cause warrants additional investigation.

Finally, the cytotoxic activity of CAR-T cells with and without inertial microfluidic processing was assessed against a target cancer reporter cell line (PC-3-Luc2). The same number of viable CAR-T cells was seeded in both cases and CAR-T cells/PC3-Luc2 ratios of 10:1, 3:1, and 1:1 were used. There was no statistically significant difference in the lytic activity between CAR-T cells processed or not ($p > 0.05$) at the 10:1 and 3:1 ratios. However, a modest but statistically significant increased lytic activity was measured for CAR-T cells processed versus unprocessed cells in inertial microfluidic devices at the 1:1 ratio ($p < 0.05$). This suggests that a cytotoxic phenotype of viable CAR-T cells is enriched in the inertial microfluidic process, which warrants further investigation. In addition, and as expected, higher cytotoxicity was measured for the transduced cells compared to the untransduced cells ($p < 0.0005$ for the 10:1 ratio, $p < 0.005$ for the 3:1 ratio, and $p < 0.05$ for the 1:1 ratio), indicating that the cytotoxic effect was specific to the CAR-T cells.

4. Conclusions

In clinical trial centers, CAR-T cells are often purified before infusion to patients. On the other hand, in the case of commercial products that are typically manufactured offsite in a central facility and shipped frozen to the treating facility, the cells are usually thawed and immediately infused back to the patient. However, these CAR-T cell products contain substantial amounts of nonviable cells (T cells and other PBMCs), as well as cryoprotectants such as DMSO. To increase the efficacy and safety of these clinical products, it would be preferable to remove these contaminates at the point of care. We demonstrated simple yet effective depletion of nonviable cells and DMSO by inertial microfluidic devices using a model CAR-T cells product currently undergoing preclinical validation. The data presented here support the feasibility and benefits of the application of cell focusing microfluidic strategies for point-of-care “polishing” of CAR-T cell products before infusion back to patients. Importantly, this could rescue “out of specification” products, thereby benefiting both patients and manufacturers. On the other hand, a potential limitation of this approach is a loss in the absolute number of CAR-T cells (≈30%), which could be an issue in products with low numbers. Additionally, the ability of inertial microfluidics to reduce the concentration of potentially detrimental T-cell phenotypes, (T-regs, T-supps, and terminally differentiated effector cells) as well as to enrich central memory and stem cell phenotypes is anticipated to have therapeutic benefits and warrants further investigation.

Supporting Information

Supporting Information is available from the Wiley Online Library or from the author.

Acknowledgements

The authors thank Carina Biotech for providing low-viability frozen CAR-T cell batches. The authors also acknowledge funding from the Australian Research Council Center of Excellence in Convergent Bio-Nano Science and Technology and the Cell Therapy Manufacturing Cooperative Research Center. This work was performed in part at the South Australian node of the Australian National Fabrication Facility under the National Collaborative Research Infrastructure Strategy to provide nano and microfabrication facilities for Australia's researchers.

Conflict of Interest

The authors declare no conflict of interest.

Data Availability Statement

Research data are not shared.

Keywords

CAR-T cell, cryoprotectant, manufacture, microfluidic, purification, viability

Received: May 30, 2021
Revised: November 15, 2021
Published online: December 8, 2021

---

[1] A. Mullard, *Nat. Rev. Drug Discovery* **2021**, *20*, 166.
[2] FDA okays second CAR-T for Kite," https://www.nature.com/articles/s41587-020-0676-z (accessed: June 2020).
[3] National Cancer Institute, FDA Approves Second CAR T-Cell Therapy, https://www.cancer.gov/news-events/cancer-currents-blog/2017/yescarta-fda-lymphoma (accessed: October 2017).
[4] S. Nam, J. Smith, G. Yang, Driving the next wave of innovation in CAR T-cell therapies | McKinsey, https://www.mckinsey.com/industries/pharmaceuticals-and-medical-products/our-insights/drivingthe-next-wave-of-innovation-in-car-t-cell-therapies (accessed: July 2019).
[5] C. Scott, CAR T-Cell Manufacturing: Challenges Remain, https://bioprocessintl.com/manufacturing/cell-therapies/challenges-andopportunities-in-car-t-cell-manufacturing/ (accessed: July 2020).
[6] D. W. Lee, N. N. Shah, *Chimeric Antigen Receptor T-Cell Therapies for Cancer E-Book: A Practical Guide*, Elsevier Health Sciences, **2019**.
[7] E. A. Chong, S. Schuster, S. Grupp, M. M. Davis, D. Siegel, S. Maude, W. Gladney, N. Frey, D. Porter, C. June, B. L. Levine, *Cytotherapy* **2019**, *21*, S19.
[8] A. Bersenev, S. Kili, *Cell Gene Ther. Insights* **2018**, *4*, 1051.
[9] D. Stroncek, S. R. Panch, P. Jin, S. L. Highfill, in *CAR T-Cell: Cell Processing Laboratory Considerations in Chimeric Antigen Receptor T-Cell Therapies for Cancer* (Eds: D. W. Lee, N. N. Shah), Elsevier, **2020**, pp. 17–28.
[10] K. L. Rock, H. Kono, *Annu. Rev. Pathol.: Mech. Dis.* **2008**, *3*, 99.
[11] B. Kollerup Madsen, M. Hilscher, D. Zetner, J. Rosenberg, *F1000Research* **2019**, *7*, 1746.
[12] K. Ikeda, H. Ohto, Y. Okuyama, M. Yamada-Fujiwara, H. Kanamori, S. Fujiwara, K. Muroi, T. Mori, K. Kasama, T. Iseki, T. Nagamura-Inoue, N. Fujii, T. Ashida, K. Kameda, J. Kanda, A. Hirose, T. Takahashi, K. Nagai, K. Minakawa, R. Tanosaki, *Transfus. Med. Rev.* **2018**, *32*, 186.
[13] W. F. Davidson, C. R. Parish, *J. Immunol. Methods* **1975**, *7*, 291.
[14] R. Hanamsagar, T. Reizis, M. Chamberlain, R. Marcus, F. O. Nestle, E. de Rinaldis, V. Savova, *Sci. Rep.* **2020**, *10*, 2219.
[15] Y.-R. Liou, Y.-H. Wang, C.-Y. Lee, P.-C. Li, *PLoS One* **2015**, *10*, e0125036.
[16] Y. Yildizhan, N. Erdem, M. Islam, R. Martinez-Duarte, M. Elitas, *Sensors* **2017**, *17*, 2691.
[17] N. Tottori, T. Nisisako, J. Park, Y. Yanagida, T. Hatsuzawa, *Biomicrofluidics* **2016**, *10*, 014125.
[18] M. C. Zalis, J. F. Reyes, P. Augustsson, S. Holmqvist, L. Roybon, T. Laurell, T. Deierborg, *Integr. Biol.* **2016**, *8*, 332.
[19] M. Islam, H. Brink, S. Blanche, C. DiPrete, T. Bongiorno, N. Stone, A. Liu, A. Philip, G. Wang, W. Lam, A. Alexeev, E. K. Waller, T. Sulchek, *Sci. Rep.* **2017**, *7*, 1997.
[20] T. Kwon, R. Yao, J.-F. P. Hamel, J. Han, *Lab Chip* **2018**, *18*, 2826.
[21] M. Winter, T. Hardy, M. Rezaei, V. Nguyen, D. Zander-Fox, M. E. Warkiani, B. Thierry, *Adv. Mater. Technol.* **2018**, *3*, 1800066.
[22] N. Nivedita, P. Ligrani, I. Papautsky, *Sci. Rep.* **2017**, *7*, 44072.
[23] M. E. Warkiani, B. L. Khoo, D. S.-W. Tan, A. A. S. Bhagat, W.-T. Lim, Y. S. Yap, S. C. Lee, R. A. Soo, J. Han, C. T. Lim, *Analyst* **2014**, *139*, 3245.
[24] B. L. Khoo, M. E. Warkiani, D. S.-W. Tan, A. A. S. Bhagat, D. Irwin, D. P. Lau, A. S. T. Lim, K. H. Lim, S. S. Krisna, W.-T. Lim, Y. S. Yap, S. C. Lee, R. A. Soo, J. Han, C. T. Lim, *PLoS One* **2014**, *9*, e99409.
[25] N. Nivedita, I. Papautsky, *Biomicrofluidics* **2013**, *7*, 054101.
[26] D. D. Carlo, D. Irimia, R. G. Tompkins, M. Toner, *Proc. Natl. Acad. Sci. USA* **2007**, *104*, 18892.
[27] N. Convery, N. Gadegaard, *Micro Nano Eng.* **2019**, *2*, 76.
[28] C. Mata, E. K. Longmire, D. H. McKenna, K. K. Glass, A. Hubel, *Microfluid. Nanofluid.* **2008**, *5*, 529.
[29] J. Hanna, A. Hubel, E. Lemke, *Biotechnol. Bioeng.* **2012**, *109*, 2316.
[30] X. Ye, H. Liu, Y. Ding, H. Li, B. Lu, *Microelectron. Eng.* **2009**, *86*, 310.
[31] A. A. S. Bhagat, S. S. Kuntaegowdanahalli, I. Papautsky, *Lab Chip* **2008**, *8*, 1906.
[32] S. Elmore, *Toxicol. Pathol.* **2007**, *35*, 495.
[33] G. Pawelec, D. Sansom, A. Rehbein, M. Adibzadeh, I. Beckman, *Exp. Gerontol.* **1996**, *31*, 655.
[34] J. G. Gribben, G. J. Freeman, V. A. Boussiotis, P. Rennert, C. L. Jellis, E. Greenfield, M. Barber, V. A. Restivo, X. Ke, G. S. Gray, *Proc. Natl. Acad. Sci. USA* **1995**, *92*, 811.
[35] S. T. Ju, D. J. Panka, H. Cui, R. Ettinger, M. el-Khatib, D. H. Sherr, B. Z. Stanger, A. Marshak-Rothstein, *Nature* **1995**, *373*, 444.
[36] M. Salmon, D. Pilling, N. J. Borthwick, N. Viner, G. Janossy, P. A. Bacon, A. N. Akbar, *Eur. J. Immunol.* **1994**, *24*, 892.
[37] E. Guzniczak, O. Otto, G. Whyte, N. Willoughby, M. Jimenez, H. Bridle, *Lab Chip* **2020**, *20*, 614.
[38] FDA, Package-Insert—KYMRIAH.pdf, https://www.fda.gov/files/vaccines%2C%20blood%20%26%20biologics/published/Package-Insert-KYMRIAH.pdf (accessed: December 2020).
[39] R. Li, R. Johnson, G. Yu, D. H. Mckenna, A. Hubel, *Cytotherapy* **2019**, *21*, 943.
[40] R. K. Iyer, P. A. Bowles, H. Kim, A. Dulgar-Tulloch, *Front. Med.* **2018**, *5*, 150.
[41] K. Hornberger, G. Yu, D. McKenna, A. Hubel, *Transfus. Med. Hemotherapy* **2019**, *46*, 188.
[42] Ç. A. Akkök, M. R. Holte, J. M. Tangen, B. Østenstad, Ø. Bruserud, *Transfusion* **2009**, *49*, 354.
[43] H. Amini, W. Lee, D. D. Carlo, *Lab Chip* **2014**, *14*, 2739.
[44] New South Wales Government, *Standards for Paediatric Intravenous Fluids: NSW Health*, 2nd ed., NSW Kids and Families, North Sydney, NSW **2014**.
[45] NICE Clinical Guidance, *Intravenous Fluid Therapy in Adults in Hospital*, National Institute for Health and Care Excellence (NICE), London **2013**.
[46] M. A. Holliday, W. E. Segar, *Pediatrics* **1957**, *19*, 823.
[47] T. K. Gregory, J. G. Berdeja, K. K. Patel, S. A. Ali, A. D. Cohen, C. Costello, E. M. Ostertag, N. de Silva, D. J. Shedlock, M. Resler, M. A. Spear, R. Z. Orlowski, *Cancer Res* **2018**, *78*, CT130.

[48] J. A. Fraietta, S. F. Lacey, E. J. Orlando, I. Pruteanu-Malinici, M. Gohil, S. Lundh, A. C. Boesteanu, Y. Wang, R. S. O'Connor, W.-T. Hwang, E. Pequignot, D. E. Ambrose, C. Zhang, N. Wilcox, F. Bedoya, C. Dorfmeier, F. Chen, L. Tian, H. Parakandi, M. Gupta, R. M. Young, F. B. Johnson, I. Kulikovskaya, L. Liu, J. Xu, S. H. Kassim, M. M. Davis, B. L. Levine, N. V. Frey, D. L. Siegel, et al., *Nat. Med.* **2018**, *24*, 563.

[49] J. A. Fraietta, C. L. Nobles, M. A. Sammons, S. Lundh, S. A. Carty, T. Reich, A. P. Cogdill, J. J. D. Morrissette, J. E. DeNizio, S. Reddy, Y. Hwang, M. Gohil, I. Kulikovskaya, F. Nazimuddin, M. Gupta, F. Chen, J. K. Everett, K. A. Alexander, E. Lin-Shiao, M. H. Gee, X. Liu, R. M. Young, D. Ambrose, Y. Wang, J. Xu, M. S. Jordan, K. T. Marcucci, B. L. Levine, K. C. Garcia, Y. Zhao, et al., *Nature* **2018**, *558*, 307.

[50] E. Lugli, M. H. Dominguez, L. Gattinoni, P. K. Chattopadhyay, D. L. Bolton, K. Song, N. R. Klatt, J. M. Brenchley, M. Vaccari, E. Gostick, D. A. Price, T. A. Waldmann, N. P. Restifo, G. Franchini, M. Roederer, *J. Clin. Invest.* **2013**, *123*, 594.

[51] T. Gargett, N. Truong, L. M. Ebert, W. Yu, M. P. Brown, *Cytotherapy* **2019**, *21*, 593.

[52] S. A. Carty, M. Gohil, L. B. Banks, R. M. Cotton, M. E. Johnson, E. Stelekati, A. D. Wells, E. J. Wherry, G. A. Koretzky, M. S. Jordan, *J. Immunol.* **2018**, *200*, 82.

[53] Y. Xu, M. Zhang, C. A. Ramos, A. Durett, E. Liu, O. Dakhova, H. Liu, C. J. Creighton, A. P. Gee, H. E. Heslop, C. M. Rooney, B. Savoldo, G. Dotti, *Blood* **2014**, *123*, 3750.

[54] L. Gattinoni, X.-S. Zhong, D. C. Palmer, Y. Ji, C. S. Hinrichs, Z. Yu, C. Wrzesinski, A. Boni, L. Cassard, L. M. Garvin, C. M. Paulos, P. Muranski, N. P. Restifo, *Nat. Med.* **2009**, *15*, 808.

[55] D. Sommermeyer, M. Hudecek, P. L. Kosasih, T. Gogishvili, D. G. Maloney, C. J. Turtle, S. R. Riddell, *Leukemia* **2016**, *30*, 492.

[56] M. Onda, K. Kobayashi, I. Pastan, *Proc. Natl. Acad. Sci. USA* **2019**, *116*, 4575.

[57] C. M. Paluskievicz, X. Cao, R. Abdi, P. Zheng, Y. Liu, J. S. Bromberg, *Front. Immunol.* **2019**, *10*, 2453.

[58] A. Tanaka, S. Sakaguchi, *Cell Res.* **2017**, *27*, 109.

[59] W. L. Byrne, K. H. G. Mills, J. A. Lederer, G. C. O'Sullivan, *Cancer Res.* **2011**, *71*, 6915.

[60] S. M. Pollack, R. L. Jones, E. A. Farrar, I. P. Lai, S. M. Lee, J. Cao, V. G. Pillarisetty, B. L. Hoch, A. Gullett, M. Bleakley, E. U. Conrad, J. F. Eary, K. C. Shibuya, E. H. Warren, J. N. Carstens, S. Heimfeld, S. R. Riddell, C. Yee, *J. Immunother. Cancer* **2014**, *2*, 36.

[61] A.-M. Rasmussen, G. Borelli, H. J. Hoel, K. Lislerud, G. Gaudernack, G. Kvalheim, T. Aarvak, *J. Immunol. Methods* **2010**, *355*, 52.

[62] P. Attia, D. J. Powell, A. V. Maker, R. J. Kreitman, I. Pastan, S. A. Rosenberg, *J. Immunother. (Hagerstown Md 1997)* **2006**, *29*, 208.

[63] S. Patrick, GPB Scientific Announces Additional Growth Financing to Support Commercialization of Curate Cell Processing System for Next-Generation Cell & Gene Therapies," https://www.businesswire.com/news/home/20210527005144/en/GPB-Scientific-Announces-Additional-Growth-Financing-to-Support-Commercialization-of-Curate%E2%84%A2-Cell-Processing-System-for-Next-Generation-Cell-Gene-Therapies (accessed: June 2021).

[64] G. Dutton, Cell Therapy Speed and Efficiency Driven by Draper's New Way of Thinking, https://www.biospace.com/article/cell-therapy-speed-and-efficiency-driven-by-draper-s-new-way-ofthinking/ (accessed: February 2021).